Nondegenerate four-wave mixing in gold nanocomposites formed by ion implantation

V. P. Safonov,* Jane G. Zhu,† N. N. Lepeshkin, R. L. Armstrong, V. M. Shalaev, and Z. C. Ying

New Mexico State University, Department of Physics
Las Cruces, NM 88003

C. W. White and R. A. Zuhr

Oak Ridge National Laboratory, Solid State Division, Oak Ridge, TN 37831

ABSTRACT

Nondegenerate four-wave mixing technique has been used to investigate the third-order nonlinear susceptibility for nanocomposite material with Au nanocrystals formed inside a SiO_2 glass matrix. High concentrations of encapsulated Au nanocrystals are formed by implantation of Au^+ ions into fused silica glass substrates and thermal annealing. The size distribution and the depth profiles of the Au nanoparticles can be controlled by the implantation dose, energy and annealing temperatures. The high value of the third-order susceptibility $\sim (0.26\text{-}1.3)\times10^{-7}$ esu was found in the range of the frequency detunings $\Delta(1/\lambda) \leq 28$ cm^{-1} near the surface plasmon resonance. Two characteristic relaxation times, 0.66 ps and 5.3 ps, have been extracted from the detuning curve of the third-order susceptibility as the probe-beam frequency changes and the pump-beam frequency fixed at the plasmon resonance. The first relaxation time was attributed to electron-phonon relaxation, and the second to thermal diffusion to the host medium. The efficient nondegenerate conversion is attractive for optical processing.

Keywords: Optical nonlinearity, nondegenerate four-wave mixing, gold nanoparticles, nanocomposite, ion implantation

INTRODUCTION

Metal nanocomposites possess high optical nonlinearities with short response times [1-12]. Large third-order nonlinear optical susceptibility, $\chi^{(3)}$, has been reported for nanocomposites with gold [1-8], silver [1,8-10], copper [10,11], and tin [12] nanoparticles. High values of the susceptibility ($\chi^{(3)}$ up to 10^{-6} esu [12]) are the result of large enhancement of the local fields in metal particles at the surface plasmon resonance and of the high hyper-polarizabilities of metal particles [1]. The mechanisms contributing to the third-order polarizability of nanoparticles for the degenerate four-wave mixing (DFWM) process include the saturation of the interband transition [4], the saturation of the absorption of the electron gas confined inside the particle [3,4,13], and the Fermi smearing or hot electron contribution [4]. For gold particles, the dominant contribution to DFWM at $\lambda = 530$ nm was found to be of the hot electron mechanism, *i.e.*, the electron redistribution due to the optical excitation of electrons

* Also with Institute of Automation and Electrometry SB RAS, Novosibirsk, 630090, Russia.
† Corresponding author. Electronic Mail: jzhu@nmsu.edu

Part of the SPIE Conference on Switchable Materials and Flat Panel Displays
Denver, Colorado • July 1999
SPIE Vol. 3788 • 0277-786X/99/$10.00

and the subsequent relaxation [4]. Laser heating of the crystal lattice in gold nanoparticles also contributes to the nonlinearity [14].

The response time of the cubic nonlinearity is often measured using the pulse delay technique in DFWM experiments [1-7,10,11,14,15]. It has been found that there are fast and slow relaxation processes, and the fast decay time is typically in picoseconds or less. The recent investigations of electron dynamics in metal films and nanoparticles using femtosecond pulses revealed femtosecond and picosecond relaxation processes. The decay times were found to depend on the probability of the electron scattering on the nonthermal electron distribution during the early stages of the electron gas internal thermalization, and on the electron temperature T_e and lattice temperature T_i after the thermalization [16-19]. The role of specific relaxation processes in the nonlinear conversion of laser waves requires further studies.

To increase the susceptibility, one could (a) aggregate nanoparticles to form fractals, which will increase the local field enhancement in the red and infrared regions [8,15], or (b) increase the volume fraction of metal particles in a sample [5-7,9-11], which can increase the total nonlinearity substantially. Stained glass prepared by melting, for example, can only have low concentration of metal particles due to the chemistry. It has been shown that high concentrations of nanocrystals can be achieved by ion implantation of high doses [5,6,11,12,20].

In this paper we report the investigation of degenerate and nondegenerate four-wave mixing in gold composites formed by ion implantation of SiO_2. Information on the time characteristics of the nonlinear material can be obtained from FWM by tuning the probe-beam wavelength [2,21]. The efficient nondegenerate conversion is attractive for optical processing. The relation of the observed data to relaxation processes in gold particles is also discussed.

EXPERIMENTAL

Our samples were prepared by implantation of Au^+ ions into Corning fused silica substrates. The sizes and size distribution of Au nanocrystals are functions of the implantation and annealing conditions [22]. In general, implantation at an elevated temperature or with a high dose leads to larger nanocrystals. For the sample used in this paper, the implantation energy was 2.75 MeV with a dose of 1.5×10^{17} ions/cm^2. The substrate was heated to 400°C during implantation to facilitate the formation of Au nanocrystals. The implanted Au concentration profile was measured by the Rutherford backscattering (RBS). The optical properties were studied by linear optical transmission and nonlinear optical measurements of degenerate and nondegenerate FWM.

The absolute value of the cubic susceptibility of gold particles in silica at the surface plasmon resonance was measured by a two-beam configuration of the FWM. Figure 1 depicts schematically the interaction of two coherent beams in a thin nonlinear medium, a diffracted beam is generated by the refractive index grating induced by the interference grating of the two incident beams [23], where ω_1, ω_2, and ω_3 are the frequencies of the pump, probe and signal waves respectively. We used an optical parametric oscillator (Spectra Physics MOPO-730) as the source of the tunable probe wave ω_2 with spectral width of less than 0.2 cm^{-1}. The narrow-band pump wave ω_1 was the frequency-doubled output of a Nd:YAG laser. The pulse duration was 4 ns for the ω_2 beam and 8 ns for the ω_1 beam. The diameters of the beams were about 2 mm. The two beams had the same linear polarization. The intensity of the probe beam, I_2, was usually less than one half of the pump intensity, I_1. These two beams crossed upon the sample at a relatively small angle (~ 5°). For DFWM, both the pump and probe beams were at the same wavelength that was tunable using the MOPO laser.

The signal beam at frequency $\omega_3 = 2\omega_1 - \omega_2$ came out in the direction, $\mathbf{k}_3$, nearly symmetric to the probe wave-vector, $\mathbf{k}_2$, with respect to the pump wave vector, $\mathbf{k}_1$. A Tektronix 2467B oscilloscope, a video camera, a computer system, fast photodiodes and neutral-density filters were used to measure the conversion efficiency for FWM, $\eta = I_3/I_2$, where I_3 is the intensity of the signal beam.

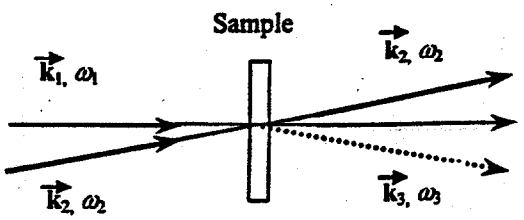

Fig. 1. Schematic diagram of forward four-wave mixing in a nonlinear thin-film sample, showing the mixing of beam 1 and 2 to provide gain in the beam-3 direction.

RESULTS AND DISCUSSIONS

The implanted Au concentration profile, measured by RBS, is shown in Fig. 2. The gold particles are distributed over a region of about 1 μm peaked at 0.9 μm from the surface. The full width at half maximum of the distribution is 0.45 μm. Investigations by cross-sectional transmission electron microscopy have showed that the average diameter of the gold particles in the sample is ~ 6 nm [22]. At the high concentration region, a few large Au particles have sizes of almost 10 nm. At the low concentration regions, the Au particles are about a few nanometers in sizes. The gold volume fraction p is estimated to be 7% in the implanted region. More details on the ion implantation of Au at different temperatures and doses can be found in ref. [22].

The absorption spectrum of the sample measured with a spectrophotometer is shown in Fig. 3. The peak of the surface plasmon absorption is at $\lambda_p = 520$ nm and has full-width at half-maximum $\Delta\lambda_p =$ 100 nm, which is close to the typical value for 6 nm Au particles [4]. The strong absorption in the short wavelength range is attributed to defect centers in SiO_2 induced by the ion implantation and interband transitions in gold.

It is observed in the FWM experiment that the intensity of the signal beam I_3 is proportional to $I_1^2 I_2$ when the intensities of the incident beams I_1 and I_2 are less than 2 MW/cm^2. At higher incident intensities, the signal beam intensity has showed saturation. Pulses with intensity more than 6 MW/cm^2 induce persistent bleaching of the sample. The experiments described below are carried out below the saturation intensities. Taking into account that our medium is absorbing and the frequency detuning range $|\lambda_1 - \lambda_2| << \Delta\lambda_p$, we can calculate the absolute value of $\chi^{(3)}(\omega_3)$ from the following equation:

$$|\chi^{(3)}(\omega_3)| = \frac{n^2 c \lambda_3}{24\pi^3} \cdot \frac{\alpha}{(1-T)\sqrt{T}} \cdot \frac{\sqrt{\eta}}{I_1},$$

where α is the absorption coefficient, $T = e^{-\alpha l}$ is the transmittance, λ_3 is the wavelength of the signal beam, n is the refractive index, and c is the speed of light in vacuum [12]. The values of α, T, and n are taken at the pump wavelength λ_1.

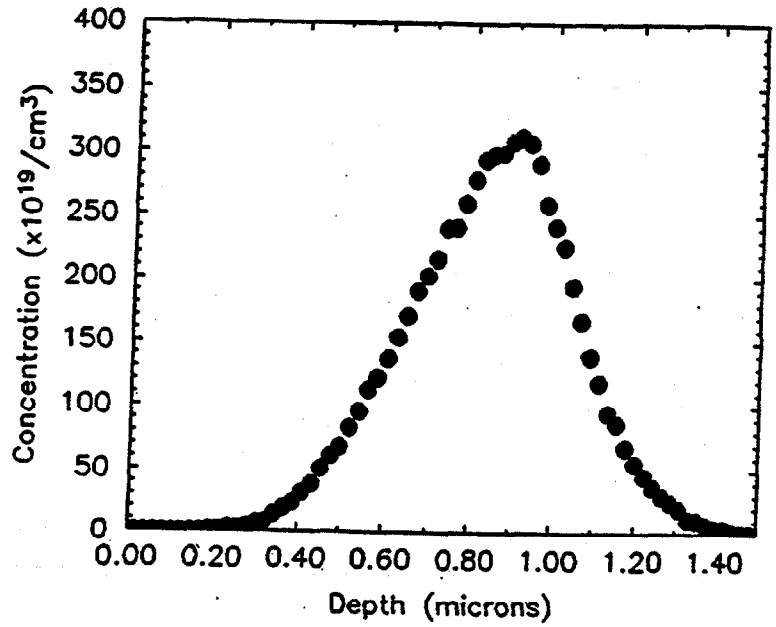

Fig. 2. Concentration profile of Au implanted into SiO_2 matrix measured by RBS.

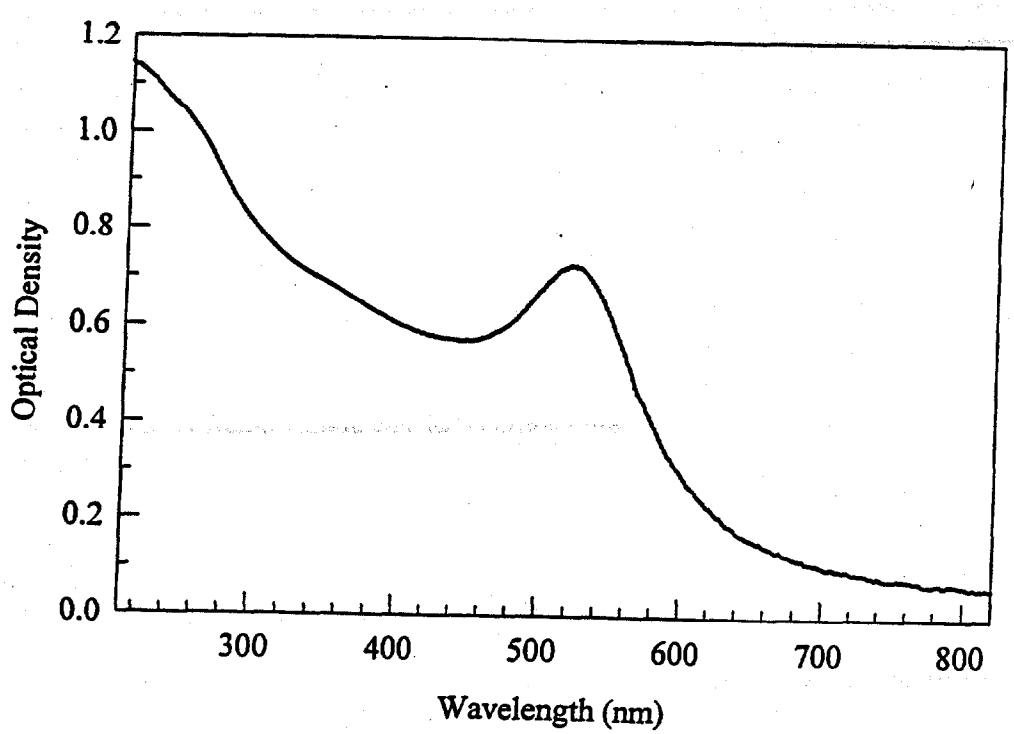

Fig. 3. Absorption spectrum of the Au implanted glass sample.

Degenerate four-wave mixing

For the DFWM at $\lambda_1 = \lambda_2 = 532.1$ nm and $I_1 = 1.9$ MW/cm^2, we have measured $|\chi^{(3)}| = 1.3 \times 10^{-7}$ esu. This value is several orders of magnitude larger than those measured for DFWM in the low-concentration gold colloid solution [1] and gold-doped glass [4], and it is also larger than that previously reported for ion implanted samples measured with picosecond pulses [5]. The corresponding susceptibility of gold particles $\chi_m^{(3)}$, which describes the nonlinear response to the internal field [1,2,4], is $\chi_m^{(3)} = \chi^{(3)}/(pf_1^2|f_1|^2)$, where p is the metal volume fraction and f_1 the ratio between the internal field E_1 and external field E_0. For 6-nm particles, $|f_1|$ is 1.7 [4]. The value of volume fraction in our sample is 0.07. Thus, we obtain $|\chi_m^{(3)}| = 2.2 \times 10^{-7}$ esu. This value of $\chi_m^{(3)}$ is close to the value of 1.1×10^{-7} esu obtained in [4].

The $|\chi^{(3)}|$ values measured by the DFWM method at different wavelengths is shown in Fig. 4. The spectral width of the DFWM $|\chi^{(3)}|$ is about 70 nm, which is less than the plasmon absorption peak width of 100 nm. This means that the absorption is controlled by homogeneous broadening in our sample, which may be explained by the effective medium theory [12]. An important characteristics of nonlinear medium is the figure of merit (FOM), $\chi^{(3)}/\alpha$. The measured value of FOM at $\lambda = 532$ nm is $\chi^{(3)}/\alpha = 4.5 \times 10^{-12}$ esu·cm ($\alpha = 2.8 \times 10^4$ cm^{-1}). This value is one half of the largest value reported [7], where the Au-SiO_2 film prepared by sputtering have very high Au concentrations (near the percolation threshold).

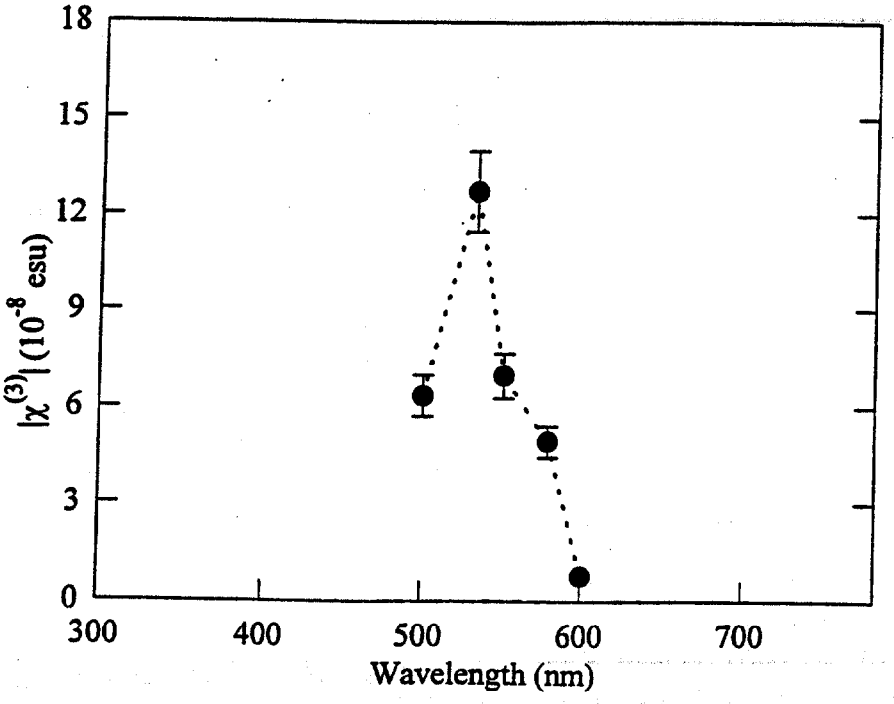

Fig. 4. $|\chi^{(3)}|$ values measured by DFWM at different wavelengths.

It is known that for certain optical switching and processing devices the refractive nonlinearity in the low absorption media is preferred. To determine contributions of the real and imaginary parts to the $\chi^{(3)}$, we have carried out z-scan measurements [24] of gold composites at λ = 532 nm. Aqueous gold colloidal solutions were prepared by the method described in [25]. It was found that the imaginary part of the $\chi^{(3)}$ dominates. One can expect a large contribution of the real part to the $\chi^{(3)}$ in the long-wavelength absorption wing of aggregated nanocomposite, which was observed for silver clusters [8].

Nondegenerate four-wave mixing

The $|\chi^{(3)}|$ values have also been measured by nondegenerate FWM through detuning of the probe beam (λ_2). Figure 5 represents the dependence of $|\chi^{(3)}(\lambda_3)|$ on the wavenumber detuning $|1/\lambda_1-1/\lambda_2|$. The data for $\lambda_1 > \lambda_2$ and $\lambda_1 < \lambda_2$ are almost symmetric. It is noteworthy that the value of $|\chi^{(3)}|$ decreases only by a factor of 5 for the wavenumber difference $|1/\lambda_1-1/\lambda_2| = 28$ cm^{-1}. The dependence of $|\chi^{(3)}|$ changes slope in the log-log scale plot at $\Omega_a = 1$ cm^{-1}, and at $\Omega_b = 8$ cm^{-1}. The slope changes from 0 to 0.2 at the first deflection point, and it changes from 0.2 to 1 at the second place.

According to the simple model of the FWM in a two-level system [21], $\chi^{(3)}$ as a function of frequency or wavenumber difference may have two deflection points. These points correspond to longitudinal (τ_1) and transverse (τ_2) relaxation times. This model is qualitatively consistent with our experiment result.

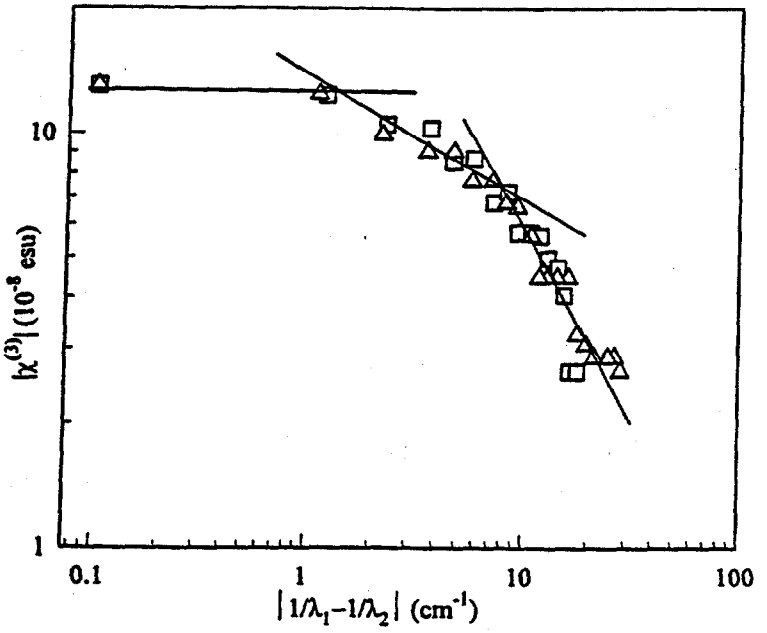

Fig. 5. Dependence of $|\chi^{(3)}(\lambda_3)|$ on the frequency difference $|1/\lambda_1-1/\lambda_2|$ (log-log plot). The □ symbols represent data for $\lambda_1 > \lambda_2$, and Δ symbols for $\lambda_1 < \lambda_2$.

To quantitatively describe the $\chi^{(3)}$ dependence on ω_3 for gold particles, a more sophisticated model was considered [2]. This model takes into account that plasmon oscillations decay nonradiatively

into a reservoir of electron and phonon energy. This thermal reservoir cools down with relaxation time τ_V. The numerical analysis [2] showed that, for short longitudinal (τ_1) and transverse (τ_2) relaxation times, the lifetime associated with energy transfer into or out of the reservoir introduces another slope change to $\chi^{(3)}$. The $\chi^{(3)}$ dispersion calculated for $\tau_V = 5.3$ ps and $\tau_2 = 3.5$ fs showed slope changes at $|1/\lambda_1 - 1/\lambda_2| = 1$ cm^{-1} and 1000 cm^{-1} [2]. No change of the slope has been observed in the FWM signal at $2.8 < |1/\lambda_1 - 1/\lambda_2| < 110$ cm^{-1} region for gold particles with a diameter of 30 nm in colloidal solution.

The characteristic times correspond to the deflection points in the detuning curve of $|\chi^{(3)}|$ are $\tau_a = (2\pi c\Omega_a)^{-1} = 5.3$ ps and $\tau_b = (2\pi c\Omega_b)^{-1} = 0.66$ ps. The time of thermal diffusivity responsible for cooling a single-particle reservoir may be estimated as $\tau_V = c_1\rho_1 r^2/3\kappa_2 = 5.4$ ps (using values of gold lattice specific heat $c_1 = 0.13$ J/g·K, density $\rho_1 = 19.3$ g/cm^3, particle radius $r = 3$ nm, and silica thermal conductivity $\kappa_2 = 0.014$ W/cm·K). The lattice temperature of gold nanoparticles in silica irradiated by 2 MW/cm^2, 10 nanosecond pulse, is evaluated as $T_i = 350$K, which is approximately equal to the electron temperature. For the thermally excited quasiparticles in the nonthermal electron model [16] at the characteristic temperatures of 300-600K, the electron-electron collision time is equal to the electron-phonon energy relaxation time, $\tau_{ep} = \gamma T_i/g = 0.77$ ps , where $\gamma = 66$ J/m^{3}K^2 (electron specific heat is $c_e = \gamma T_e$), and electron-phonon coupling coefficient $g = 3 \times 10^{16}$ W/m^3·K. Considering the good agreement between τ_a, τ_b and the estimated τ_V, τ_{ep}, we attribute the deflection points measured in our experiments to the characteristic times of the thermal diffusivity from a gold particle to a host medium, $\tau_V = \tau_a = 5.3$ ps, and to electron-phonon energy relaxation time, $\tau_{ep} = \tau_b = 0.66$ ps.

CONCLUSIONS

Large nonlinear susceptibility, $|\chi^{(3)}| > 10^{-7}$ esu, was observed in the nanocomposite of gold imbedded in glass formed by the ion implantation technique. RBS measurement shows that Au was implanted within the 1 μm region near the surface. The third-order susceptibility has been measured using both the degenerate and nondegenerate four-wave mixing method. High values of $\chi^{(3)} \sim (0.26\text{-}1.3)\times 10^{-7}$ esu were found in the range of the frequency detunings $|\Delta(\frac{1}{\lambda})| \leq 28$ cm^{-1} near the surface plasmon resonance. The response and relaxation times have been determined based on the detuning curve. The $\chi^{(3)}(\omega_3)$ dispersion is governed by the characteristic times of 0.66 ps, 5.3 ps, which are due to the excited electron energy loses and cooling of the nanoparticles.

ACKNOWLEDGMENTS

VPS is grateful to S.G. Rautian for stimulating discussions. This work was supported in part by NSF under grants DMR-9623663, and by RFBR grant 96-02-19331. JGZ and NNL acknowledge the partial support from Los Alamos National Laboratory (New Mexico Universities Collaborative Research) and Sandia University Research Program. Oak Ridge National Laboratory is supported by U.S. Department of Energy (DOE), under contract DE-AC05-96OR22464 with Lockheed Martin Energy Research Corp.

REFERENCES

[1] D. Richard, P. Roussignol, and C. Flytzanis, Opt. Lett. **10**, 511 (1985).

[2] E. J. Heilweil and R. M. Hochstrasser, J. Chem. Phys. **82**, 4762 (1985).
[3] F. Hache, D. Ricard, and C. Flytzanis, J. Opt. Soc. Am. **B 3**, 1647 (1986).
[4] F. Hache, D. Ricard, C. Flytzanis, and U. Kreibig, Appl. Phys. **A 47**, 347 (1988).
[5] R. H. Magruder, III, Li Yang, R. F. Haglung, Jr., C. W. White, L. Yang, R. Dorsinville, and R. R. Altano, Appl. Phys. Lett. **62**, 1730 (1993).
[6] K. Fukumi, A. Chayahara, K. Kadono, T. Sakaguchi, Y. Horino, M. Miya, K. Fujii, J. Hayakawa, and M. Satou, J. Appl. Phys. **75**, 3075 (1994).
[7] H. B. Liao, R. F. Xiao, J. S. Fu, P. Yu. G. K. L. Wong, and P. Sheng, Appl. Phys. Lett. **70**, 1 (1997); H. B. Liao, R. F. Xiao, H. Wang, K. S. Wong, and G. K. L. Wong, Appl. Phys. Lett. **72**, 1817 (1998).
[8] Yu. E. Danilova, V. P. Drachev, S. V. Perminov, and V. P. Safonov, Bull. Russian Acad. Sci. Physics **60**, 342 (1996).
[9] S. G. Rautian, V. P. Safonov, P. A. Chubakov, V. M. Shalaev, and M. I. Stockman, JETP Lett. **47**, 243 (1988).
[10] K. Uchida, S. Kaneko, S. Omi, C. Hate, H. Tanji, Y. Asahara, A. J. Ikushima, T. Tokizaki, and A. Nakamura, J. Opt. Soc. Am. B **11**, 1236 (1994).
[11] L. Yang, K. Becker, F. M. Smith, R. H. Magruder, III, R. F. Haglund, Jr., L. Yang, R. Dorsinville, R. R. Alfano, and R. A. Zuhr, J. Opt. Soc. Am. B **11**, 457 (1994).
[12] Y. Takeda, T. Hioki, T. Motohiro, and S. Noda, Appl. Phys. Lett. **63**, 3420 (1993).
[13] S. G. Rautian, JETP **85**, 451 (1997).
[14] M. J. Bloemer, J. W. Haus, P. R. Ashley, J. Opt. Soc. Am. B **7**, 790 (1990).
[15] A. V. Butenko, P. A. Chubakov, Yu. E. Danilova, S. V. Karpov, A. K. Popov, S. G. Rautian, V. P. Safonov, V. V. Slabko, V. M. Shalaev, and M. I. Stockman, Z. Phys. D. **17**, 283 (1990).
[16] R. H. M. Groeneveld, R. Sprik, and A. Lagendijk, Phys. Rev. B **51**, 11433(1995).
[17] C. Suarez, W. E. Bron, and T. Juhasz, Phys. Rev. Lett. **75**, 4536(1995).
[18] M. Perner, P. Post, U. Lemmer, G. von Plessen, J. Feldmann, U. Becker, M. Mennig, M. Schmitt, and H. Schmidt, Phys. Rev. Lett. **78**, 2192 (1997).
[19] N. Del. Fatti, R. Boufannais, and C. Flytzanis, Phys. Rev. Lett. **81**, 922 (1998).
[20] J. G. Zhu, C. W. White, J. D. Budai, S. P. Withrow, and Y. Chen, J. Appl. Phys. **78**, 4386 (1995).
[21] T. Yajima, Opt. Commun. **14**, 378 (1975).
[22] C. W. White, D. S. Zhou, J. D. Budai, R. A. Zuhr, R. H. Magruder, and D. H. Osborne, Mat. Res. Soc. Symp. Proc. **316**, 499 (1994).
[23] I. C. Khoo and T. H. Liu, Phys. Rev. A **39**, 4036 (1989).
[24] M. Sheik-Bahae, A. A. Said, T.-H. Wei, D. J. Hagan, and E. W. Van Stryland, IEEE J. Quantum Electron. **26**, 760 (1990).
[25] G. Frens, Nature **241**, 20 (1973).